Alfvén waves in Reversed-Field Pinch and Tokamak Ohmic plasmas: nonlinear 3D MHD modelling and comparison with RFX-mod

A. Kryzhanovskyy[1,3], **D. Bonfiglio**[1,2], **S. Cappello**[1,2], **M. Veranda**[1] **and M. Zuin**[1,2]

[1] Consorzio RFX (CNR, ENEA, INFN, Università di Padova, Acciaierie Venete SpA), C.so Stati Uniti 4, 35127 Padova, Italy
[2] CNR- ISTP Padova, Italy
[3] CRF – University of Padova, Italy

E-mail: artur.kryzhanovskyy@igi.cnr.it; daniele.bonfiglio@igi.cnr.it

Abstract. The properties and possible triggering mechanisms of Alfvén waves in the reversed-field pinch (RFP) and circular tokamak configurations are discussed in the framework of nonlinear 3D MHD modelling. Numerical simulations are performed with the SpeCyl code (S. Cappello and D. Biskamp 1996 *Nuclear Fusion*) that solves the equations of the viscoresistive MHD model in cylindrical geometry. Configurations with increasing level of complexity are analyzed. First, single-wave numerical solutions have been compared with analytical ones in the simplest case of a uniform axial magnetic field: an excellent agreement is obtained for both the shear Alfvén wave (SAW) and the compressional Alfvén eigenmodes (CAEs). Then, tokamak and RFP configurations have been studied. Phenomena such as phase mixing of SAW, resonant absorption of CAEs and the appearance of the global Alfvén eigenmode (GAE) are described. Finally, the fully 3D RFP case with the typical sawtoothing activity has been investigated, showing for the first time in nonlinear RFP simulations the excitation of Alfvén waves by magnetic reconnection events. Modeling results appear to be consistent with the experimental characterization of Alfvénic activity observed in RFX-mod.

Keywords: Alfvén waves, RFP, tokamak, MHD, SAW, CAE, GAE.

1. Introduction

Alfvén waves are ubiquitous in astrophysical and laboratory plasmas [1]. In magnetically confined fusion plasmas, alpha particles and energetic particles from neutral beam injection (NBI) can destabilize Alfvén eigenmodes (AEs), driven in the spectral gaps of the shear Alfvén continua [2,3,4]. The presence of these modes in the plasma leads to larger alpha particle losses before thermalization if the drift, bounce or transit frequencies of the energetic particles are resonant with the mode frequency [5]. This increases the requirements for operations in self-sustained ignited plasmas and can decrease NBI heating efficiency [6]. On the other hand, if the mode frequency is small, the interaction between background plasma and energetic particles may lead to a stabilizing effect (nonresonant limit) [7,8]. The fact that Alfvén modes are frequently observed in tokamak, stellarator and reversed field pinch (RFP) plasmas suggests that they could be used as a diagnostic of plasma equilibrium parameters. This MHD spetroscopy has shown how measurements of Alfvén waves mode structures can provide information on plasma parameters at particular points in the plasma [9]: in particular, the safety factor can be determined locally in several regions of the plasma using measurement of excited AEs. In principle, AEs could also provide the basis for a plasma heating scheme as supplementary heating of fusion plasmas [10,11,12]. Indeed, heating by Alfven waves excitation is one of the common mechanisms envisaged for solar corona heating [13,14,15]. Alfvén waves are also thought to play a possible role during tokamak disruptions, as recently investigated both theoretically [16] and experimentally [17]. The scientific challenge in this context is to find the proper balance between desired and detrimental effects of the various MHD modes, to develop methods and tools for active feedback control of Alfvén modes [18] and identify new issues that may arise in approaching the ignition margin.

Alfvén waves in fusion plasmas can appear in a vast zoology of modes. Variations in the Alfvén speed produce frequency gaps associated with different Alfvén eigenmode families (n is the toroidal mode and m the poloidal mode), including [2]: toroidicity induced Alfvén eigenmodes (TAE) [19,20] that arise due to coupling of m with $m+1$ modes, helicity induced Alfvén eigenmodes (HAE) [21,22,23] arising from coupling combinations of n and m modes, beta induced Alfvén eigenmodes (BAE) [24,25] driven by compressibility effects, reversed-shear Alfvén eigenmodes (RSAE) [26,27] due to local maxima/minima in the rotational transform profile, island-induced Alfvén eigenmodes (IAE) [28,2] arising from a helical coupling of harmonics due to the magnetic island etc.. Most commonly, these AEs have been observed in the presence of energetic ions in the MeV energy range, with velocities comparable with Alfvén velocity directed along the magnetic field lines, which can satisfy conditions of effective resonance and energy exchange between Alfvén waves [29]. However, modes with Alfvénic frequency scaling have also been detected during Ohmic discharges in a number of tokamak experiments, like TFTR [30], ASDEX Upgrade [31] and MAST [32]. The dominant toroidal mode number for Alfvén eigenmodes in Ohmic plasmas was generally found to be $n = 0$. Excitation and detection of Alfvén waves in Ohmic plasmas is not much studied and understood as currently the research on this subject is mostly centered (as already mentioned) around the excitation of AE by fast particles with velocities of the order of Alfvén speed, produced by neutral-beam injection (NBI), ion cyclotron resonance heating (ICRH), or even fusion born alpha particles, through the inverse Landau damping mechanism. Some possible mechanisms for the excitation of AEs in tokamaks in Ohmic regime have been investigated in Ref. [33], where a correlation between high-frequency mode activity and relatively long-timescale MHD events in the plasma, such as internal reconnection events (IREs) or edge localized modes (ELMs), was proposed.

Similarly, a variety of Alfvénic eigenmodes have been observed in the magnetic spectra of RFP plasmas in the past years, in experimental devices such as Extrap-T2R [34], RFX-mod [35] and MST [36,37,38]. Alfvénic eigenmodes observed in MST are mainly found to be induced by NBI. Therefore, several recent papers addressed the MST observations by modeling and analytical study of energetic particle driven AEs in RFPs [36,39,40]. On the other hand, AEs in Extrap-T2R and RFX-mod have been observed in Ohmic discharges. In particular, two distinct types of AEs with dominant toroidal mode number $n = 0$ have been detected in RFX-mod Ohmic discharges: Alfvén modes present during the whole plasma discharge duration (and related with quasi-periodic spontaneous magnetic reconnection processes) [35]; and Alfvén modes observed only for plasma currents $I_p >$ 1.5 MA and associated to helical states with improved confinement [41] that spontaneously and intermittently emerge through the nonlinear saturation of resistive-kink/tearing modes in RFX-mod plasmas [42,43]. The driving mechanism for AEs in RFX-mod was speculated [35] to be provided by the supra-thermal ions tails generated by the spontaneous magnetic reconnections during sawtooth crashes [44,45,46], where large magnetic energy is released [47] but a modeling study directly addressing these findings in Ohmic-heated RFP plasmas was lacking so far.

The first goal of this paper is to provide, by means of non-linear 3D MHD numerical simulations performed with the cylindrical code SpeCyl [48], a possible explanation of the experimental observation of AEs in RFX-mod Ohmic plasmas. This has led, as a more general result, to the identification of an excitation mechanism for the AEs based on velocity perturbations self-consistently induced by periodic magnetic reconnection events. With the support

from theoretical dispersion relations we will suggest the identification of AEs experimentally observed during the whole discharge as a global shear and a compressional eigenmode. This is achieved after a thorough discussion of simpler cases, which provide renewed occasion for numerical code benchmarking. The possible origin of the second type of AEs (those observed only during helical states and not reproduced in the present nonlinear MHD modeling) is discussed in the final remarks.

The paper is organized as follows. In section 2 the employed numerical model is described. The nonlinear 3D MHD cylindrical code SpeCyl has been used to analyze configurations with increasing level of complexity, and the obtained numerical results are presented in sections 3 (2D single wave cases) and 4 (fully 3D cases). First of all, in section 3.1, numerical solutions have been compared with analytical ones in the most simple case of a uniform axial magnetic field: an excellent agreement is obtained for both the shear Alfvén wave (SAW) and the compressional Alfvén eigenmodes (CAEs). Then in sections 3.2 and 3.3, circular tokamak and RFP configurations have been studied. Phenomena such as phase mixing of SAW, resonant absorption of CAEs and the appearance of the GAE are reported. Finally, in section 4, the fully 3D RFP case with realistic magnetic reconnection events [49] has been investigated, showing for the first time in nonlinear RFP simulations the excitation of Alfvén waves by magnetic reconnection. Modelling results are in good qualitative agreement with the experimental observation of Alfvénic activity in RFX-mod, as discussed in section 5. A summary and final remarks are given in section 6.

2. MHD model and numerical setup

The simulations reported in this paper are performed in cylindrical geometry with the nonlinear visco-resistive 3D MHD code SpeCyl [48]. The code runs in constant density and zero-β approximation. SpeCyl solves the following set of visco-resistive MHD equations in dimensionless form:

$$\rho \frac{\mathrm{d}\mathbf{v}}{\mathrm{d}t} = \mathbf{J}\times\mathbf{B} + \rho\nu\nabla^2\mathbf{v} \tag{1}$$

$$\frac{\partial \mathbf{B}}{\partial t} = -\nabla\times\mathbf{E} \tag{2}$$

$$\mathbf{E} = \eta\mathbf{J} - \mathbf{v}\times\mathbf{B} \tag{3}$$

$$\nabla\times\mathbf{B} = \mathbf{J} \tag{4}$$

$$\nabla\cdot\mathbf{B} = 0. \tag{5}$$

Where t is the time, ρ the constant fluid density, $\mathbf{v}$ the plasma velocity, $\mathbf{B}$ the magnetic field, $\mathbf{E}$ the electric field and $\mathbf{J}$ the current density. The resistivity η and kinematic viscosity ν are assumed to be constant and uniform, unless stated otherwise. Lenghts are normalized to the cylinder minor radius a, density to the on-axis ion mass density ρ_0, magnetic field to the initial on-axis magnetic field $B^{0,0}$, velocity to the on-axis Alfvén velocity $v_A = B^{0,0}/\sqrt{\mu_0\rho_0}$ and time to the Alfvén time $\tau_A = a/v_A$. Moreover, in these units, η is the inverse Lundquist number, $\eta = \tau_A/\tau_R \equiv S^{-1}$, and ν corresponds to the inverse viscous Lundquist number, $\nu = \tau_A/\tau_V \equiv M^{-1}$, where τ_R and τ_V are the resistive and viscous time scales. The nonlinear verification benchmark between SpeCyl and another MHD code, called PIXIE3D [50], demonstrated an excellent agreement between the two codes in their common limit of application, showing that both codes solve the nonlinear MHD equations with high accuracy and reliability [51]. Adding a finite pressure and the possible presence of fast particles, and considering a toroidal geometry would allow the modeling of additional important effects active in Alfvén waves destabilization. In particular, toroidal Alfvén eigenmodes (TAEs) and slow compressional waves are allowed by inclusion of toroidal geometry and finite beta, respectively. However, the Alfvénic modes considered in this paper (in particular the global and the fast compressional eigenmodes) do not necessary require finite beta or toroidal effects to be present. In addition, the MHD dynamics of the RFP configuration is mostly current driven [49,52], and finite beta effects are usually subdominant. Therefore the employed model, while relatively simple, is qualitatively adequate to the scope of this paper. On the other hand, the nonlinear approach of the SpeCyl code makes possible to study not only the linear stability properties of AEs (as mostly done in the literature, with the notable exception of hybrid MHD-kinetic codes such as M3D [53], XHMGC [54,55], HYMAGIC [56,57] and MEGA [58], or kinetic extension of MHD codes such as NIMROD [59] or JOREK [60,61]) but also to consider the self-consistent nonlinear dynamics including mode damping and nonlinear coupling between different modes.

The numerical solution of the above equations is solved adopting a spectral formulation in periodic cylindrical coordinates (r,θ,z) with $r\in[0:a]$, $\theta\in[0:2\pi]$ and $z\in[0:2\pi R_0]$ where R_0 is given by the aspect ratio of the periodic cylinder. In this paper we use $R_0/a = 4$ to mimic the aspect ratio of the RFX-mod experimental device. A finite difference staggered mesh is used in the radial coordinate.

The plasma boundary conditions at $r = a$ are chosen to represent an ideal, i.e. perfectly conducting, shell. The magnetic field is tangent to the shell, while the electric field is perpendicular to it. Plasma flow is taken to be vanishing at $r = a$. This implies the conservation in time of the total magnetic flux Φ_0. The BCs can also be generalized to admit a magnetic field not purely tangent, with an imposed radial component, i.e. helical boundary conditions on $B_r(a)$ (as described in Ref. [62]).

In Figure 1 are shown, in order of increasing complexity, all the equilibrium configurations that are considered in nonlinear MHD simulations. For each configuration the equilibrium (mean-field) magnetic field,

density profiles and the expected Alfvén wave solutions for selected (m,n) modes (according to the ideal MHD theoretical model), are shown. The expected Alfvén waves spectra were obtained from their dispersion relations in cylindrical geometry derived from linearized ideal MHD model ($\eta = \nu = 0$) in the cold plasma approximation (pressure $p = 0$) and perfectly conducting shell conditions. The ideal MHD model is well suited for the analysis of SpeCyl simulations, despite SpeCyl being a visco-resistive code. In fact, according to the theory [1], dissipative terms related to resistivity and viscosity only introduce a damping effect that cause the waves to decay in time, without actually affecting their frequency spectrum, which is what we are mainly focused on in this paper.

3. Single wave benchmark cases

For each simulation, we will test the presence of Alfvén waves and characterize their properties (such as frequency spectra and nonlinear dynamics) by computing the Fast Fourier Transform (FFT) or Continuous Wavelet Transfrom (CWT) of simulation data, depending on whether the analysis is done on signals that vary their frequency slowly or quickly in time, respectively. In particular, FFTs are performed over time windows spanning $500\,\tau_A$. This value is chosen as it is short enough for the field components not to change significantly and it allows to obtain FFTs with good frequency resolution. The computed spectra are compared with the expected ones shown in Figure 1.

Except for the time-evolving RFP configuration, for which the simulation parameters will be specified later, we used ideal boundary conditions, a radial resolution of 256 points and a single Fourier harmonic in the angular directions, with periodicity (m,n) specified for each simulation case. The dissipation parameters are $S = 10^6$ and $M = 10^6$ respectively. The simulation time step is $10^{-4}\,\tau_A$, and fields were saved every $0.1\,\tau_A$. Moreover, Alfvén waves are excited starting from a stable equilibrium configuration by applying a small initial perturbation to the velocity field.

3.1. Equilibrium configurations with uniform axial magnetic field: uniform and hollow density cases

Uniform density case. In the case of a uniform magnetic field, the shear and compressional Alfvén waves are decoupled and hence can be excited separately depending on the initially perturbed component of the velocity field. We consider the mode $(m,n) = (0,1)$, with initial $v_\theta^{0,1}$ perturbation, or with initial $v_r^{0,1}$ perturbation. We choose this mode as this is the simplest case that presents both SAW and CAE solutions.

We start with initial velocity perturbation on the ***azimuthal component*** $v_\theta^{0,1}$, with radial profile given by

$$v_\theta^{0,1}(r) = \varepsilon r(1-r), \tag{6}$$

where $\varepsilon = 10^{-6}$. We can see from Figure 2a that in this case only the $B_\theta^{0,1}$ and the $v_\theta^{0,1}$ components are finite. Which component is excited by the initial perturbation depends on the MHD coupling between $\mathbf{B}^{0,1}$ and $\mathbf{v}^{0,1}$ components. The time traces of $B_\theta^{0,1}$ and $v_\theta^{0,1}$ at mid radius appear as sinusoids with a period ΔT such that about 10 cycles are observed in a range of $250\,\tau_A$. It is therefore expected that by doing the FFT of these time signals a single frequency $\omega\tau_A = 2\pi\tau_A/\Delta T \simeq 2\pi/25 \simeq 0.25$ would be obtained. In fact, doing the FFT in the interval $t \in [0, 500\,\tau_A]$ as shown in Figure 2b, we obtain a spectrum with a well defined frequency centered on the expected value. This is the SAW expected from ideal MHD model in cylindrical geometry, given by the following dispersion relation

$$\omega^2 - v_A^2 k_z^2 = 0, \tag{7}$$

where $k_z^2 = n^2/R_0^2$. As we can see in the verification benchmark reported in Figure 3a, we have an excellent agreement regarding both the frequency spectrum of the mode and its radial shape.

Let us see now what we obtain from a simulation in which the ***radial component*** of velocity is perturbed instead of the azimuthal one. As we can see from Figure 2c in this case we obtain three non-zero components, $B_r^{0,1}$, $B_z^{0,1}$ and $v_r^{0,1}$. We again recognize a wave pattern but this time it does not correspond to a simple sinusoidal wave. This is confirmed by Figure 2d, in which multiple harmonics are observed. The frequency spectrum shows the CAEs with their nodes, where the Alfvénic oscillations have zero amplitude. The expected spectrum of CAEs from ideal MHD model in cylindrical geometry is given by the following dispersion relation

$$\omega_{mj}^2 = v_A^2 \left(k_z^2 + \frac{{\chi_{mj}}^2}{a^2} \right), \tag{8}$$

with $j = 1,2,3\ldots$ and where χ_{mj} is the $j-$th root of the first derivative of the Bessel function of order m (namely $m = 0$ in this case). Note that in this paper we are considering only the fast compressional mode, as SpeCyl runs in zero-β approximation, that is no plasma pressure ($p = 0 \Rightarrow c_s^2 = \gamma p_0/\rho_0 = 0$). Indeed by assuming $c_s^2 = 0$ the slow compressional mode frequency is always zero. Again we have an excellent agreement between the simulation spectrum and the analytical solution as can be seen from Figure 3b. A slow decay of the waves amplitude, due to the finite resistivity and viscosity in the SpeCyl code, would be observed by looking at the fields evolution during a longer time window. However, resistivy and viscosity do not alter the frequencies of Alfvén waves with respect to the ideal MHD solutions, as discussed for instance in [1].

The above analysis is applied to similar single-mode simulations with various mode numbers $m = 0$ and n chosen between $n = 0$ and $n = 6$ for both $v_r^{0,1}$ and $v_\theta^{0,1}$ initial perturbations in order to further verify the analytical dispersion relations for CAEs and SAW. As can be seen

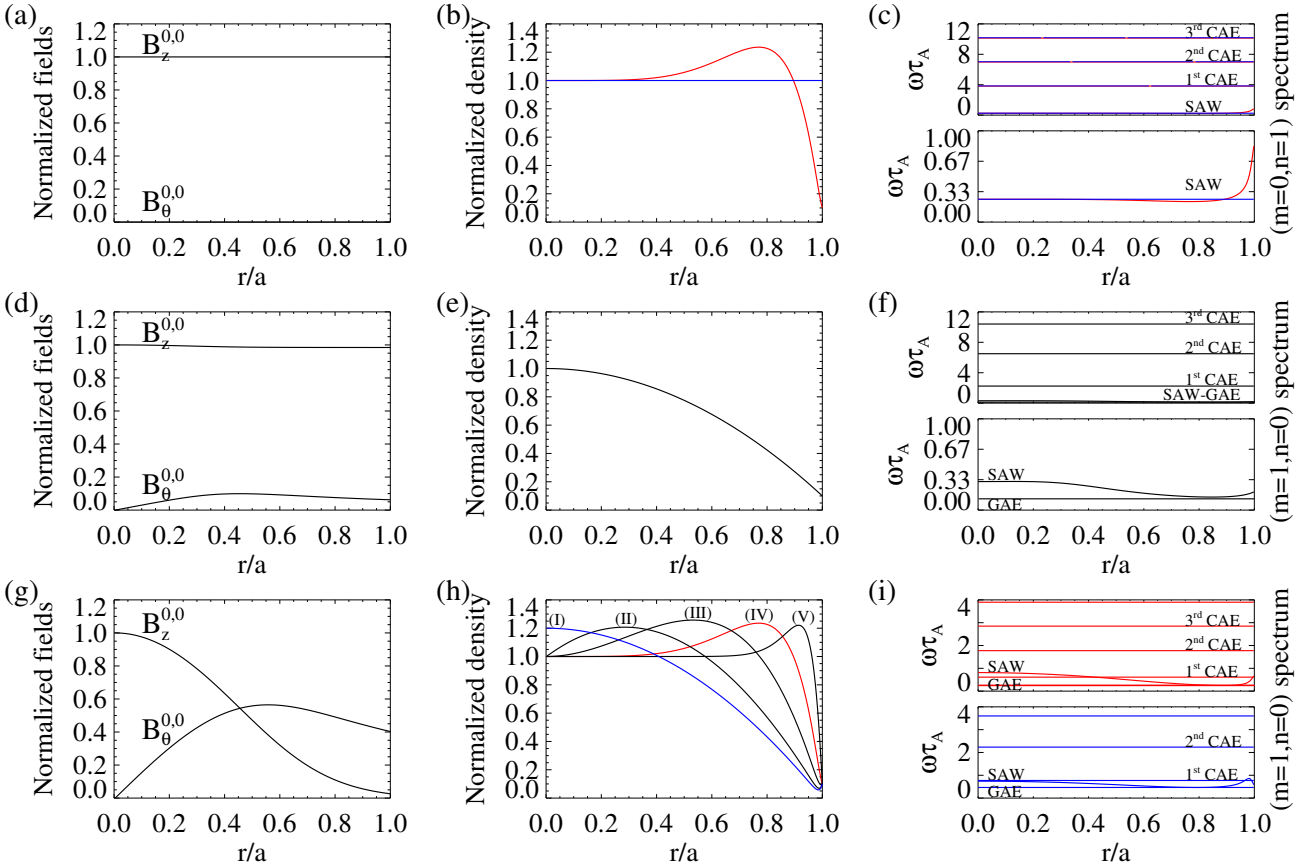

Figure 1: Different equilibrium configurations considered in this study and corresponding Alfvén spectra. Normalized magnetic field profiles, normalized density profiles and the resulting analytical solutions of the Alfvén waves spectra are shown in the first, second and third column, respectively. Each row represents a class of equilibrium configurations. The equilibrium with uniform axial magnetic field is shown in the first row (with analysed Fourier mode $(m,n) = (0,1)$), with uniform equilibrium density and corresponding analytical SAW and CAE spectra depicted in blue, and RFX-mod hollow density profile and corresponding spectra in red. The tokamak equilibrium and the RFP-like equilibrium are shown in the second and third row, respectively. In the last two cases, the analysed Fourier mode is $(m,n) = (1,0)$. For the latter, the five density profiles considered in this study, together with the corresponding spectra for two selected density profiles, are reported with different colors.

from Figure 4 the values of the CAEs and SAW frequencies (solid dots) from simulations are in complete agreement with the theoretical model (solid lines).

Hollow density case. Let us now consider the previous simulations with $(m,n) = (0,1)$ perturbed mode but in the presence of an RFX-mod-like hollow density profile. By analysing the simulation with initial velocity perturbation on the ***radial component***, the resulting frequency spectrum (not shown here) is qualitatively very similar to the one with the uniform density in Figure 2d, with the CAEs frequencies just slightly shifted downward. An additional basic phenomenon of Alfvén waves physics is observed, on the other hand, in the simulation with the perturbation on the ***azimuthal velocity component***. We can see from Figure 5b that the frequency spectrum is much different from the one with uniform density shown in Figure 2b. Now we have a SAW characterized by a continuous spectrum with a frequency that depends on the radius, with a profile resembling the inverse of the density profile (red solid line in Figure 1b). This is expected of course, as the Alfvén frequency is inversely proportional to the square root of the density, which can be seen from SAW dispersion relation in non-uniform plasmas, called also *continuous shear Alfvén wave spectrum* or the *Alfvén continuum*

$$\omega(r) = |\mathbf{k}\cdot\mathbf{v}_A| = \frac{|k_\theta B_\theta^{0,0} + k_z B_z^{0,0}|}{\sqrt{\mu_0\rho_0}}, \tag{9}$$

where $k_\theta = m/r$ and $k_z = n/R_0$.

We can now look at the time evolution of the SAW spectrum during the nonlinear MHD simulation. To do this, we perform the FFT of simulation data on a moving time window, with same duration of $500\,\tau_A$ but increasing initial time, as marked with square brackets in Figure 5a. By looking at the temporal evolution of the SAW spectrum

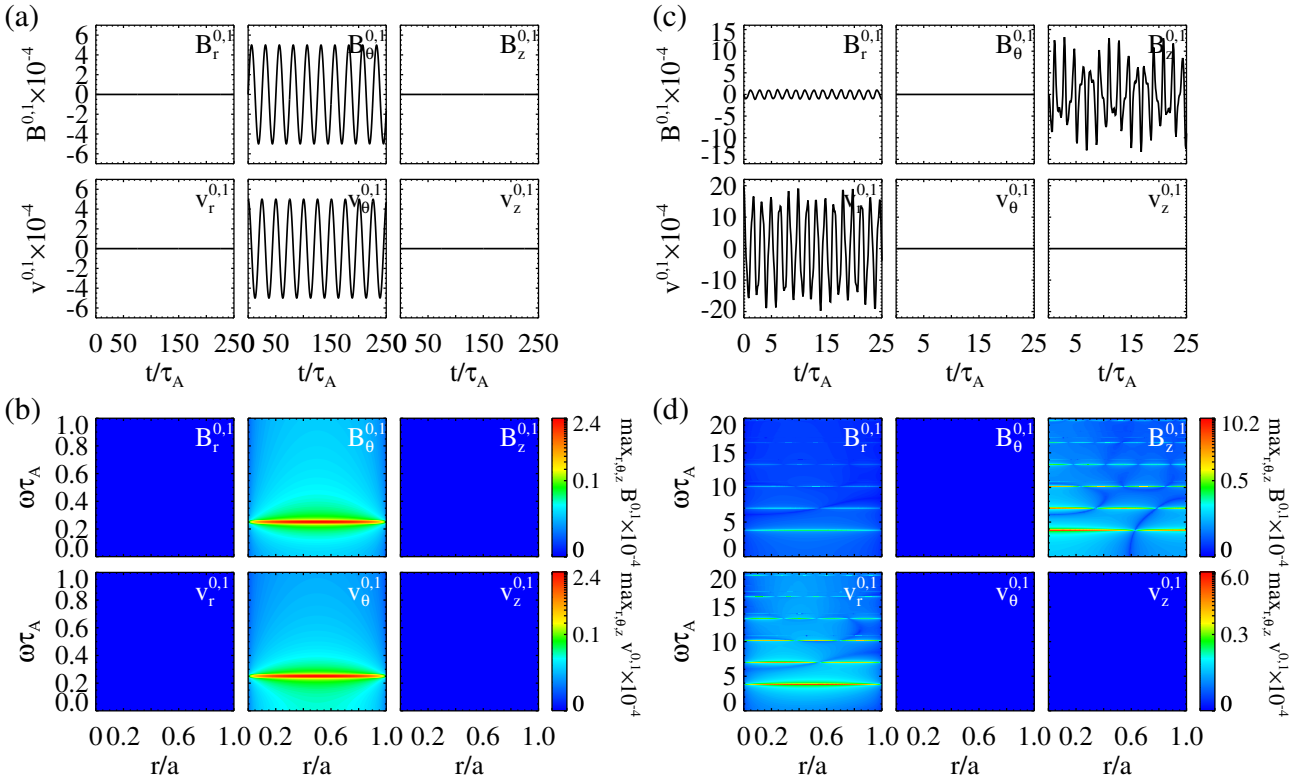

Figure 2: Results of numerical simulations with uniform axial magnetic field and density, and perturbation of the $(m,n) = (0,1)$ mode. In the first column, the simulazion with initial $v_\theta^{0,1}$ is reported. a) Time traces of $\mathbf{v}^{0,1}$ and $\mathbf{B}^{1,0}$ normalized fields components are shown at a fixed radius $r/a = 0.5$. b) The corresponding frequency spectra of $\mathbf{v}^{0,1}$ and $\mathbf{B}^{0,1}$ normalized components are shown as a function of radius, computed for the time window $t \in [0, 500\tau_A]$. The color scale, used for the contours in this paper, is not linear but follows a power law, which is necessary to detect higher order harmonics, and it refers to the absolute value of the spectral amplitude. In the second column, the same quantities are shown for the simulation with initial $v_r^{0,1}$ perturbation.

in Figure 5b, one can observe that the amplitude of the wave is damped very quickly at the radial positions with stronger radial gradient of the Alfvén frequency, while it remains almost constant close to the extremes of the $\omega(r)$ profile, i.e. the regions around $r/a = 0.25$ and 0.75. This is consistent with the phase mixing phenomenon, due to which the Alfvén wave tends to be more rapidly damped in the regions with spatially variable Alfvén frequency [1,2]. This damping mechanism acts on top of the damping due to the visco-resistive dissipation, which instead occurs uniformly throughout the plasma volume since the dissipation coefficients (resistivity and viscosity) are assigned to be uniform in these SpeCyl simulations.

3.2. Tokamak equilibrium configuration

Now we consider the first case with a non-uniform magnetic field. This configuration is a numerical solution of the 1D zero-β paramagnetic pinch equilibrium equations, discussed for instance in [51]. An azimuthal field (net plasma current) is added to the weakly non-uniform axial field, giving rise to a tokamak-like equilibrium configuration as shown in Figure 1d. It corresponds to a paramagnetic pinch equilibrium with aspect ratio $R_0/a = 4$, uniform resistivity and an applied axial electric field given by $\alpha_0 = 0.625$ (the parameter α_0 is defined in [51] and corresponds to the ratio between the applied electric field and the central resistivity). This is an intermediate case that we consider before moving on to the RFP configuration. For this tokamak configuration, with safety factor value in the center $q(0) = 0.8$ and at the edge $q(a) = 4.0$, we consider the case with a non-uniform bell-shaped density profile shown in Fig. 1e. From now on we consider the $(m,n) = (1,0)$ mode (instead of the $(0,1)$ mode considered in previous cases), as in RFX-mod it is one of the modes with the strongest Alfvénic activity [35], and also because this mode is the most excited by Alfvén waves in the more realistic time-evolving RFP configuration as we will see in the next sections.

By perturbing $v_r^{1,0}$ we can see in Figure 6 that now the CAEs spectrum is present also in the $B_\theta^{1,0}$, $v_\theta^{1,0}$ and $v_z^{1,0}$ components, compared with the analogous Figure 2d of the uniform field case, in which these components are not

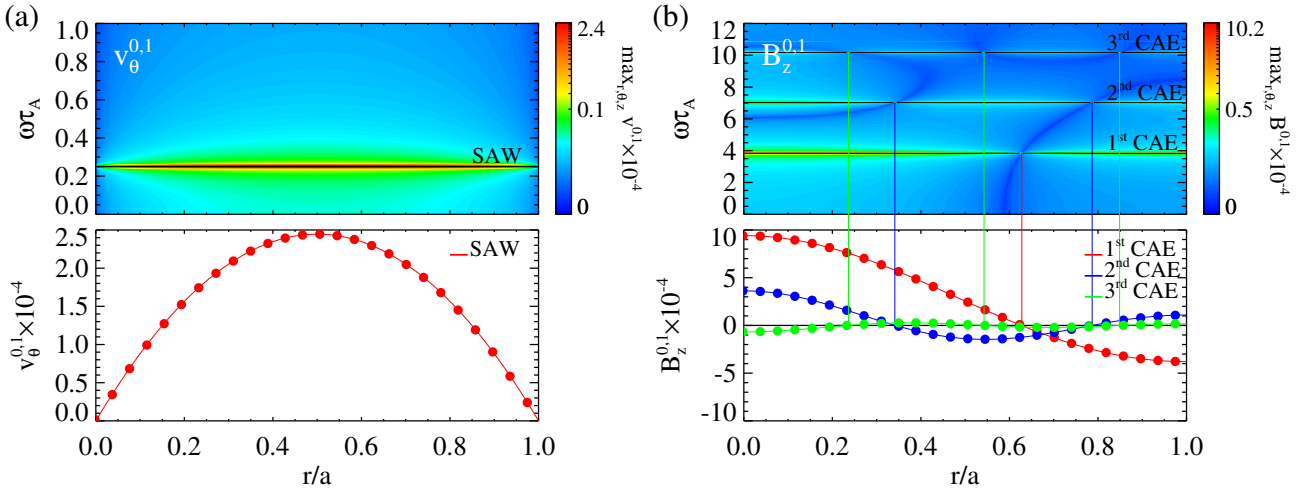

Figure 3: Verification benchmark between numerical simulations with uniform axial magnetic field and corresponding analytical spectra. a) Simulation with uniform axial magnetic field and uniform density. $(m,n) = (0,1)$ mode with initial $v_\theta^{0,1}$ perturbation. On the top panel the agreement of simulation's frequency spectrum of the $v_\theta^{0,1}$ component and the expected theoretical one given by Eq.(7) (solid black line), are shown. On the bottom panel the analytical perturbation given by Eq.(6) (solid line) is displayed together with the corresponding values from the simulation spectrum (solid dots). b) Same equilibrium configuration and analised mode as in (a) but with initial $v_r^{0,1}$ perturbation. On the top panel, the simulation frequency spectrum of the $B_z^{0,1}$ component and the corresponding analytical spectrum given by Eq.(8) (solid black lines) are shown. On the bottom panel the analytical solution (Bessel function of order $m = 0$) for the frequencies of the first three CAEs (solid lines) are displayed together with the corresponding values from the simulation spectrum (solid dots). Note that on the top panel the oscillations are shown with their absolute values, while in the bottom panel they are not.

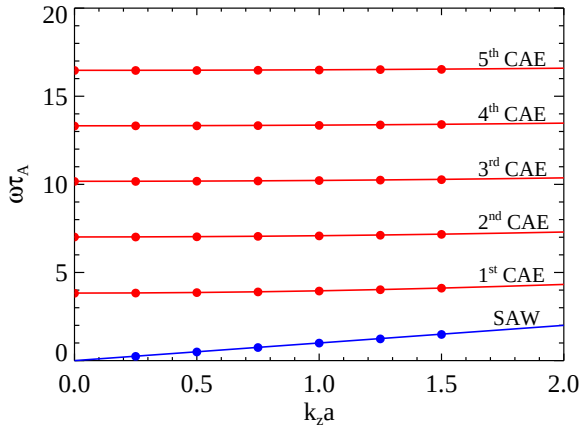

Figure 4: Verification benchmark between numerical results (solid dots) with uniform axial magnetic field and corresponding analytical spectra (solid lines). Same equilibrium configuration, and $m = 0$ analysed Fourier mode, as in Figures 2 and 3, but with different toroidal periodicities from $n = 0$ to $n = 6$. The frequency dependence on k_z wavevector component for the SAW and the first five CAEs from numerical simulations match very well the analytical solutions.

excited at all. On the other hand, the SAW is also present in all field components with similar amplitudes to the CAEs. In other words, we have a coupling of the shear and the compressional modes. This coupling is due to the fact that the wavevector **k** of the perturbation is now oblique to the magnetic field $\mathbf{B}^{0,0}$. Therefore only the perturbation in $v_r^{1,0}$ will be discussed in the following analysis. In addition, in this configuration it can be clearly seen in Figure 6b the occurrence of the global Alfvén eigenmode, which is a global mode right below the Alfvén continuum minimum (see Ref. [63]). The properties of the observed GAE will be discussed again in the context of RFP simulations in Section 3.3.

Recent studies of CAEs in tokamak plasmas were carried out in ASDEX Upgrade [64], where the modes were excited by energetic particles (NBI), and DIII-D [17], with modes excited by runaway electrons. GAEs in tokamak plasmas have been studied for instance in Refs. [65,66].

In the last panel of Fig. 6 we overplot the numerical frequency spectrum with the expected theoretical one (Figure 1f) to identify the various frequencies. A good qualitative agreement between the numerical and theoretical spectra is observed. The small discrepancy is due to the fact that now the expected CAEs frequencies are obtained in the *local* or *Wentzel-Kramers-Brillouin (WKB) approximation* as the MHD equations are no longer

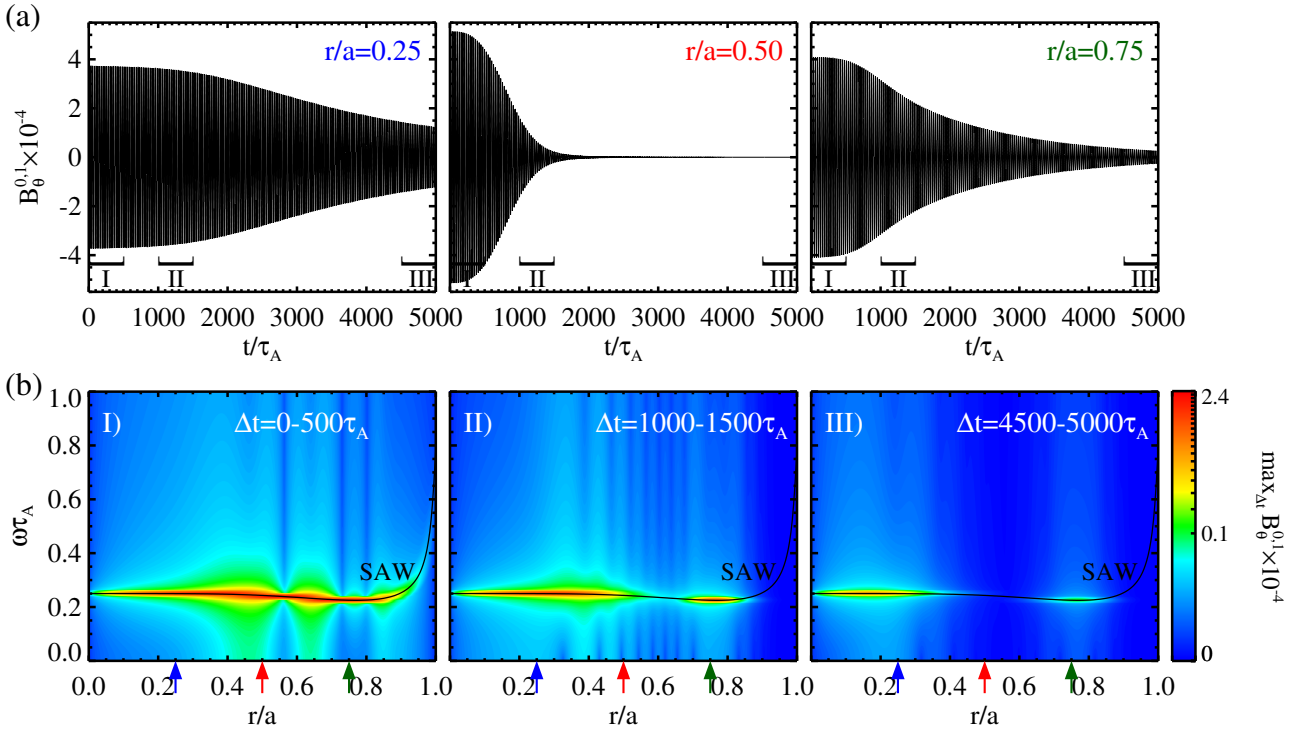

Figure 5: Temporal evolution of the continuous SAW spectrum during the simulation with uniform axial magnetic field and RFX-mod-like hollow density profile. $(m,n) = (0,1)$ mode with initial $v_\theta^{0,1}$ perturbation. a) The time traces of the normalized magnetic field component $B_\theta^{0,1}$ are shown at a fixed radius $r/a = 0.25, 0.50, 0.75$. The three time windows indicated (I, II, III), each of $500\tau_A$, are those used for the FFT in figures below. b) Time evolution of the frequency spectrum of $B_\theta^{0,1}$ at the beginning of the simulation (panels I and II) and the end of the simulation (panel III). The frequency spectrum is also superimposed with the analytical solution of the Alfvén continuum given by Eq. 9. The color coded arrows mark the radial positions considered in the above time traces of $B_\theta^{0,1}$ field component. For the corresponding movie, see supplemental material S1.

analytically solvable for CAEs in case of non-uniform plasmas [1]. The approximate analytical solution for CAEs in non-uniform plasmas is given by the following condition

$$\int_0^a \left(\frac{\omega_{mj}^2}{v_A^2(r)} - \frac{n^2}{R_0^2} \right)^{1/2} \mathrm{d}r = \chi_{mj}, \tag{10}$$

with $j = 1,2,3\ldots$ and the following constraint on ω_{mj}^2 values

$$\omega_{mj}^2 \geq \frac{n^2}{R_0^2} v_A^2(r) \quad \forall r \in [0,a]. \tag{11}$$

The GAE solution can be obtained in WKB approximation (as derived in Refs. [63]) from the following condition and it is in good agreement with the corresponding numerical spectrum

$$\int_0^a k_r \mathrm{d}r = j\pi, \tag{12}$$

with $j = 1,2,3\ldots$ and

$$k_r = \left[-\left(\frac{B_z^{0,0}}{B^{0,0}} \right)^2 \frac{1}{r} \frac{1}{\triangle} \left(\frac{\mathrm{d}}{\mathrm{d}r} \ln(\omega_A^2) + \frac{\mathrm{d}}{\mathrm{d}r} \ln \rho_0 \right) \right]^{1/2}, \tag{13}$$

where

$$\triangle \equiv \frac{\omega_A^2 - \omega_j^2}{\omega_A^2} \tag{14}$$

is the frequency separation between the GAEs and the continuum, with the following constraint on ω_j^2 values

$$\omega_j^2 < \omega_A^2(r) \quad \forall r \in [0,a]. \tag{15}$$

3.3. Paramagnetic pinch, RFP-like equilibrium configurations

We now consider the RFP-like configuration. As in the previous tokamak-like case this configuration is a numerical solution of the 1D zero-β paramagnetic pinch equilibrium equations. The lack of the axial field reversal at the edge

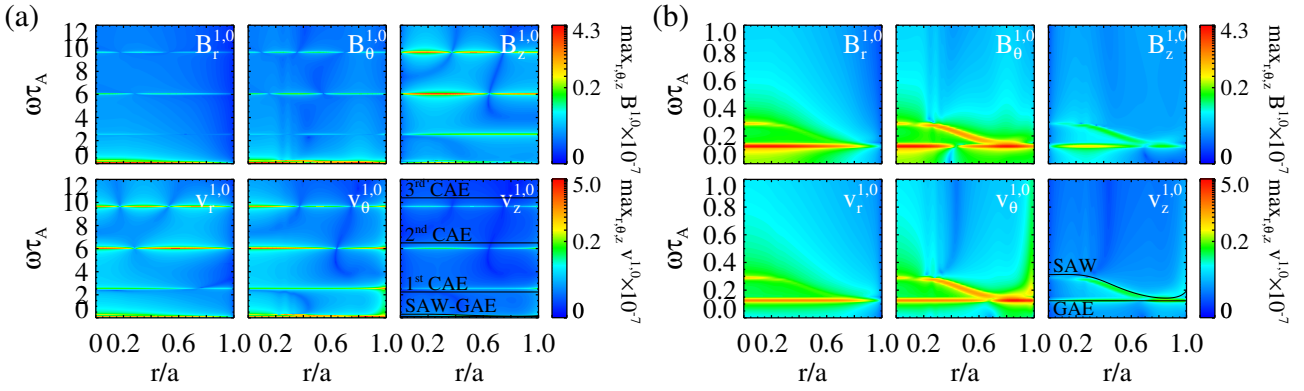

Figure 6: Results of numerical simulation with Tokamak magnetic field and bell-shaped density. $(m,n)=(1,0)$ mode with initial $v_r^{1,0}$ perturbation. a) The frequency spectra of $\mathbf{v}^{1,0}$ and $\mathbf{B}^{1,0}$ normalized fields components are shown as a function of radius, as computed for the time window $t\in[0,500\tau_A]$. b) Magnification in the frequency of the spectrum in (a) to emphasize the SAW and GAE spectra.

is just a mathematical consequence of the 1D equilibrium assumption, also known as Cowling's theorem (see also Ref. [67]). The specific RFP-like equilibrium used in this paper is shown in Figure 1g. It corresponds to a paramagnetic pinch equilibrium with aspect ratio $R_0/a=4$, uniform resistivity and $\alpha_0=3.25$. Similarly to the tokamak-like case shown in the previous section, the components of $\mathbf{v}^{1,0}$ and $\mathbf{B}^{1,0}$ fields are affected by both continuous SAW and discrete CAEs, with comparable amplitudes, so in the following simulations we will analyse only one field component, typically either the $B_z^{1,0}$ or the $v_r^{1,0}$ component.

In Figure 7, we look at the time evolution of the $B_z^{1,0}$ component with an RFX-mod like density profile. Compared to the tokamak configuration now the SAW frequency range increases while the CAE frequencies are shifted down, so that a very peculiar condition occurs due to the RFP-like magnetic field profiles: the 1^{st} CAE crosses the shear Alfvén continuum. In the first panel we overplot the numerical frequency spectrum with the expected theoretical one (Figure 1i) to identify the various frequencies. From the spectrum temporal evolution we can observe again the phase mixing of the SAW, which disappears in the first $\sim 300\,\tau_A$ (although it survives longer at the radial location of the frequency minimum due to the negligible local gradient). We also observe the resonance absorption of the 1^{st} CAE, which completely vanishes by the end of the simulation. The resonance absorption phenomenon occurs when a wave propagates in a smooth non-uniform plasma and couples with the continuous spectrum of the shear Alfvén wave, getting absorbed (and localy heating the plasma) [1,68].

In order to try to excite the GAE mode, which we expect to see as in the tokamak case, we investigate the five equilibrium density profiles shown in Figure 1h. In particular we consider density profiles with different radial positions of their peak density, going from the wall to the plasma center. Here we only examine the profile that is most efficient to excite the GAE mode, namely the density profile peaked in the center (profile (I) in Figure 1h). The temporal evolution of the frequency spectrum resulting from the SpeCyl simulation with perturbed $(m,n)=(1,0)$ mode and bell-shaped density profile is shown in Figure 8, where in the first panel we overplot the numerical spectrum with the expected theoretical one (Figure 1i) in order to identify the various frequencies. As we can see in the Figure, we observe a new global mode just below the Alfvén continuum minimum, that is the GAE. We can also see, as in the previous case, the phase mixing of the SAW and the resonance absorption of the 1^{st} CAE. Both waves disappear as before, while the GAE mode survives along the whole simulation duration. This analysis points out that the GAE mode is more easily excited with density profiles peaked near the plasma center.

4. Fully-3D time-evolving reversed-field pinch case

As the final goal of this study, we consider the case of time-evolving fully-3D RFP simulation, with quasi-periodic magnetic reconnection events associated with the typical RFP sawthooting activity, as described in the modeling studies of Refs. [49,52,69]. This is close to the experimental conditions and this analysis will make possible a direct comparison with the experimental observations in the RFX-mod device.

The nonlinear MHD simulation that is analyzed here is a continuation of the original simulation reported in Ref. [49], with same MHD spectrum but with a non-uniform RFX-mod-like hollow density profile instead of the standard uniform density profile typically used in SpeCyl. As in the previous section, fields are saved each $0.1\,\tau_A$ (a high sampling frequency suitable for the analysis

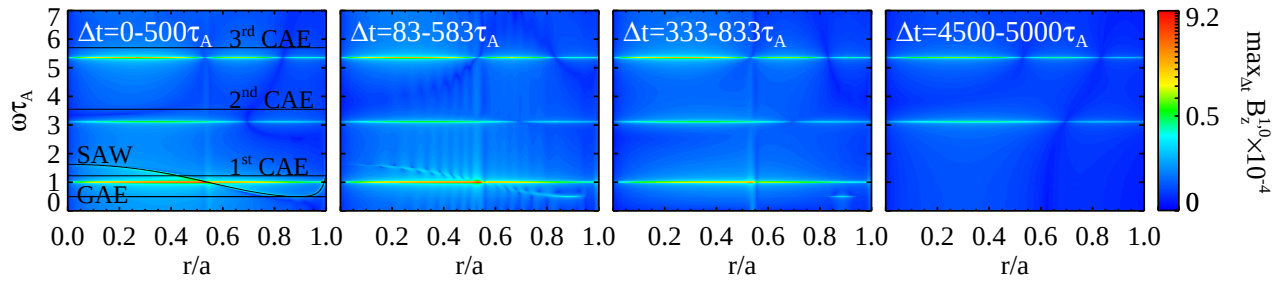

Figure 7: Temporal evolution of the spectrum of the numerical simulation with RFP-like magnetic field and hollow density profile. $(m,n) = (1,0)$ mode with initial $v_r^{1,0}$ perturbation. Time evolution of the frequency spectrum of the normalized magnetic field component $B_z^{1,0}$ at the begining of the simulation (first three panels) and the end of the simulation (last panel). In the first panel the frequency spectrum is superimposed with the expected analytical solutions for SAW, CAEs and GAE. For the corresponding movie, see supplemental material S2.

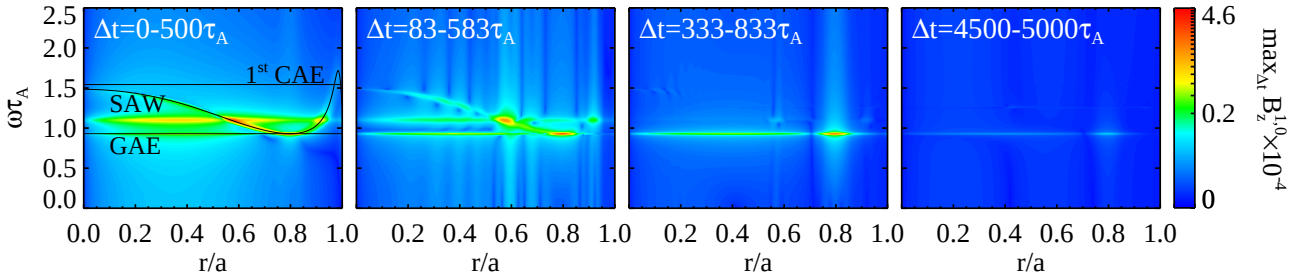

Figure 8: Temporal evolution of the spectrum of the simulation with RFP-like magnetic field and density profile peaked in the center. $(m,n) = (1,0)$ mode with initial $v_r^{1,0}$ perturbation. Time evolution of the frequency spectrum of the normalized magnetic field component $B_z^{1,0}$ at the begining of the simulation (first three panels) and the end of the simulation (last panel). In the first panel the frequency spectrum is superimposed with the expected analytical solutions for SAW, CAE and GAE. For the corresponding movie, see supplemental material S3.

of Alfvén waves) instead of each $10\tau_A$ as done in the original simulation. The time step is also reduced from $t = 5\times10^{-2}\,\tau_A$ to $t = 10^{-3}\,\tau_A$ to obtain a more accurate characterization of Alfvén modes. These differences slightly change the dynamics with respect to the original simulation, but only quantitatively and not qualitatively. As in the original simulation, a spectrum of 225 Fourier harmonics with $0 \le m \le 4$ is used, the on-axis Lundquist and viscous Lundquist numbers are set to $S = 10^6$ and $M = 10^4$, respectively, and a seed helical perturbation with $m = 1$, $n = -7$ periodicity is applied to the edge B_r to stimulate quasi-helical states in between reconnection events as discussed in Ref. [49].

The temporal evolution of the edge safety factor $q(a)$ and the normalized edge B_z amplitudes of the most active $m = 1$ modes are shown in Figure 9, for the original simulation on the left column, and for the modified one on the right. The original simulation starts from a non-reversed 1D paramagnetic pinch equilibrium. The initially positive edge safety factor $q(a)$ suddenly reverses due to the nonlinear 3D MHD activity associated to resistive-kink tearing modes (see Ref. [69]), providing the so-called dynamo mechanism (i.e. magnetic flux pumping provided by toroidal current density partially converted into poloidal one, due to kink effect). The system, then, undergoes sawtoothing oscillations exhibiting periodic magnetic reconnection events as highlighted by bursts in the MHD mode amplitudes. The new simulation starts from time $t = 3.0\times10^4\,\tau_A$ of the original simulation. We focus on two subsequent sawtoothing cycles.

We consider in particular the $(m,n) = (1,0)$ mode as in previous RFP-like cases, but a fundamental difference is that now the simulation includes many nonlinearly interacting MHD modes as shown in Fig. 9. It is also important to note that Alfvén modes in this simulation do not depend on specific details of the initial velocity perturbation. Now, each reconnection event self-consistently excites, through the associated velocity perturbation, Alfvén modes in a quasi-periodic fashion. Although in this new simulation the mean magnetic field is time evolving, such mean field is still changing much slower compared to the evolution of Alfvén waves, and therefore it can be used as before for theoretical predictions of the Alfvén modes frequency spectrum.

We now analyze for the new simulation the time evolution at fixed radius $r/a = 0.6$ of the $v_r^{1,0}$ spectrum using both the FFT and CWT techniques, as shown in Figure 10, where we also plot the time traces of the edge $B_z^{0,0}$ normalized magnetic field component and the corresponding trend of kinetic and magnetic energies. As expected, during the magnetic reconnection events, starting around $t = 3.45 \times 10^4\,\tau_A$ and $t = 3.90 \times 10^4\,\tau_A$, a rapid decrease of magnetic energy is observed while the kinetic energy has a peak. At the same time, we can observe an excitation of the frequency spectrum following the two magnetic reconnection events which lasts for some time. In particular, the frequency spectrum in time shows intense low-frequency fluctuations and also weaker discrete signals at higher frequencies (horizontal lines in the spectogram) which are particularly noticeable after the second reconnection event resulting in a much stronger velocity perturbation than the first one. It is worth mentioning that in this case with time evolving fields, the CWT technique provides better results than the FFT. In particular, the discrete frequency peaks are much more definite with the CWT analysis, and their triggering time agrees more precisely with the time of the kinetic energy peak. On the other hand, the FFT analysis provides less sharp results mainly because it is applied on a finite time window (500 τ_A in this case). The low-frequency fluctuations are due to tearing modes which dominates the dynamics of the system in this configuration. The discrete signals, on the other hand, can be identified as Alfvén modes as we will now discuss.

In Figure 11 we superimpose the frequency spectrum of the v_{1r} component, after the stronger magnetic reconnection event at $t = 3.90 \times 10^4\,\tau_A$, with the theoreticaly expected one in order to identify the various Alfvénic frequencies. We recognize the first three CAE frequencies, the first one being the most excited while the third being barely visible, and the GAE mode, which indirectly confirms the presence of the continuous SAW, being damped by phase mixing and hidden by noise from low-frequency MHD fluctuations. Note that in this case the GAE is seen with the RFX-mod-like hollow density profile, while in the RFP simulations with initial velocity perturbation (discussed in Section 3.3) it was seen only with the density profile peaked in the center. As mentioned above, we have chosen to analyse the $(m,n) = (1,0)$ harmonic as in RFX-mod it is one of the modes with the strongest Alfvénic activity [35]. This is also the case for the fully 3D simulation, as an analysis of the frequency spectra of a wide range of (m,n) modes ($0 \le m \le 2$ and $-9 \le n \le 9$) right after the magnetic reconnection events showed the strongest excitation of AEs in the $(m,n) = (1,0)$ mode. The numerical result we have obtained, showing that Alfvén waves can be excited by magnetic reconnection events, provides a theoretical confirmation of experimental observations in the RFX-mod device, where the same qualitative phenomenology (with Alfvénic fluctuations excited after reconnection events) is found.

5. Comparison with experimental observations in RFX-mod

We conclude this analysis with a comparison of numerical RFP results with experimental observations on the RFX-mod device. Experimentally five distinct peaks have been observed in the power spectrum of the magnetic fluctuations measured at the plasma edge of RFX-mod device. For convenience we name these peaks a, b, c, d and e following the increase of their frequency, from ~ 130 kHz to ~ 1 MHz. While the first three peaks (a,b,c) are present only during the Single-Helical-Axis (SHAx) states, in which the plasma is in an almost stationary quasi helical equilibrium with a single magnetic axis, the two highest frequency peaks, d and e, do not seem to be associated to any particular behavior of the dominant mode, being present during almost the full discharge duration. All of these peaks were interpreted as Alfvén waves because their frequencies scale linearly with the Alfvén velocity of the plasma, as shown in Figure 12. The RFX-mod discharges from which these data were taken are characterized by periodic magnetic reconnection events similar to the simulation case (see Ref. [41]).

We give now an interpretation of the above experimental observations, based on the results of the analysis carried out in this paper. We start by comparing the frequencies of the experimentally observed Alfvén waves (the five peaks) with the frequency spectrum of the dynamic time-evolving RFP simulation from Figure 10b. In order to do so we first need to plot the numerical frequency spectrum in physical units, as until now we have always considered dimensionless units. By taking the RFX-mod minor radius $a = 0.459$ m and a reference Alfvén speed of $v_A = 2500$ km/s (corresponding in RFX-mod to the high plasma current where all the five coherent peaks are observed), we obtain the following Alfvén time $\tau_A = a/v_A \simeq 0.2\,\mu$s. The resulting frequency spectrum in physical units is shown in Figure 13, where we indicate the Alfvénic nature of the discrete signals, identified above. On the other hand, in Figure 12 we mark the frequencies of d and e peaks corresponding to the reference Alfvén speed.

Comparing the two previous plots, we notice that the GAE and the 1^{st} CAE frequencies values appear in the same frequency range of d and e peaks, with comparable frequency separation between them. This brings us to formulate the following hypothesis on the Alfvénic nature of those peaks, namely that d corresponds to a GAE mode, while e corresponds to the 1^{st} CAE.

We can therefore speculate about the physical mechanism triggering these Alfvén waves (d and e peaks), that is they are excited by self-consistent velocity perturbation triggered by the magnetic reconnection events taking place in the plasma. This is indeed consistent with the exper-

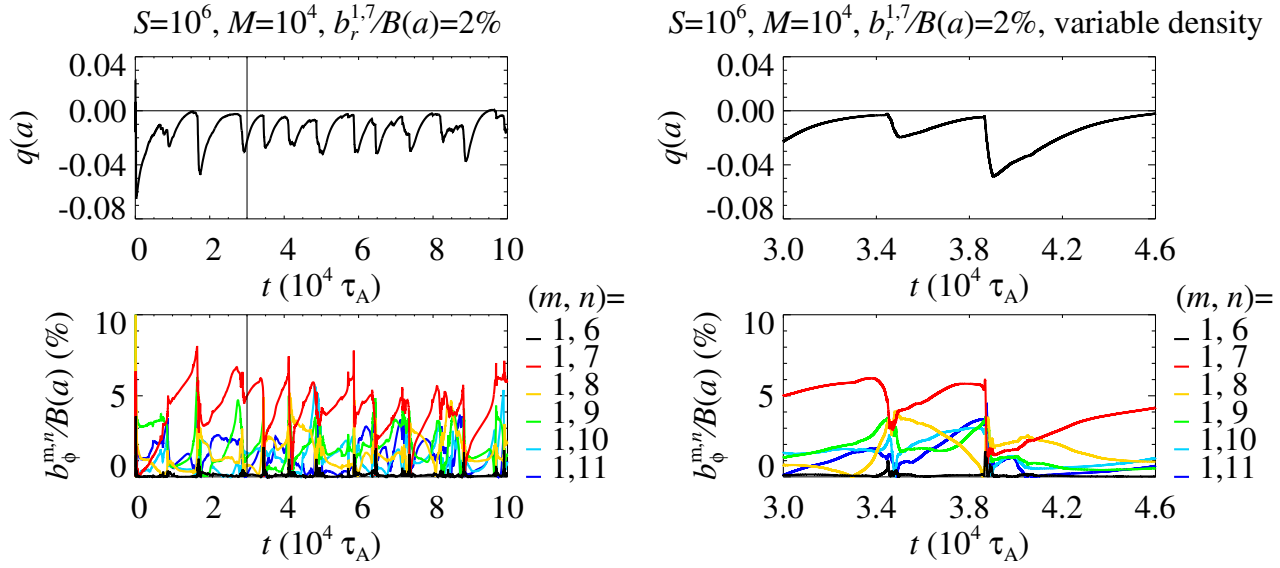

Figure 9: Time-evolving RFP configuration. In the top panels it is shown the temporal evolution of the edge $q(a)$, while in the bottom panels the edge amplitudes of the most active $m = 1$ modes (color coded) are shown as a function of time. The original simulation reported in Ref. [49] is shown in the left column, while on the right the new simulation with RFX-mod-like hollow density profile analysed in this paper is shown, starting from time $t = 3.0 \times 10^4 \tau_A$ of the original simulation and showing two subsequent magnetic reconnection events.

imental observation that the amplitude of such high frequency fluctuations nearly double during magnetic reconnection events [35].

6. Summary and final remarks

In this paper, a systematic theoretical investigation of the physics of Alfvén waves in pinch configurations, by means of analytical theory and numerical simulations based on the nonlinear 3D MHD model, has been discussed. High-frequency magnetic activity was previously reported by edge measurements in the RFX-mod device, and associated analysis showed several coherent modes clearly depending on the Alfven velocity [35]. The specific aim of this paper was to provide a theoretical description of experimental observations of AEs and their drive mechanism in RFP devices, where only ohmic heating is present.

Numerical simulations were performed with the SpeCyl code [48] that solves the equations of the viscoresistive MHD model in cylindrical geometry. The analysis started with an equilibrium configuration with uniform axial magnetic field and uniform density profile. This was the only case for which an exact analytical solution for Alfvénic modes SAW and CAE can be obtained from the theoretical models. The verification of the numerical frequency spectra with the theoretical ones showed complete agreement, thus demonstrating the applicability of the SpeCyl code as a well suited simulation tool for the study of Alfvén waves. As a second step, more complex configurations were analysed, first with non-uniform density profile and then with non-uniform magnetic fields (Tokamak-like configuration). In these cases the comparison with the theoretical models was done employing the WKB approximation for the CAEs, as these modes do not possess an analytic solution for non uniform plasmas. The good agreement between numerical and theoretical spectra in this cases allowed us to be confident on the interpretation of numerical spectra for non-uniform cases. Furthermore the theoretically predicted phenomena for those cases, namely the damping mechanism of the continuous SAW, phase mixing, and the coupling between the SAW and CAEs, were observed. As a further step we analysed a simplified RFP-like equilibrium configuration of the magnetic fields, first with uniform and then with different variable density profiles. This case proved useful to show that in the RFP configuration a peculiar condition occurs, that is the direct coupling between the SAW continuum and the 1^{st} CAE, unlike in the tokamak configuration in which the compressional modes are usually neglected, as they are much higher in frequency than the shear mode. Besides modes coupling and phase mixing, an additional phenomenon was observed in this case, the resonance absorption, which damps any compressional mode directly coupled to the continuous spectrum of the shear Alfvén wave.

The last step was the analysis of a fully-3D time-dependent realistic RFP simulations. These simulations are modeled after real RFX-mod discharges and display a self-consistent MHD dynamics characterised by periodic magnetic reconnection events. This part was crucial

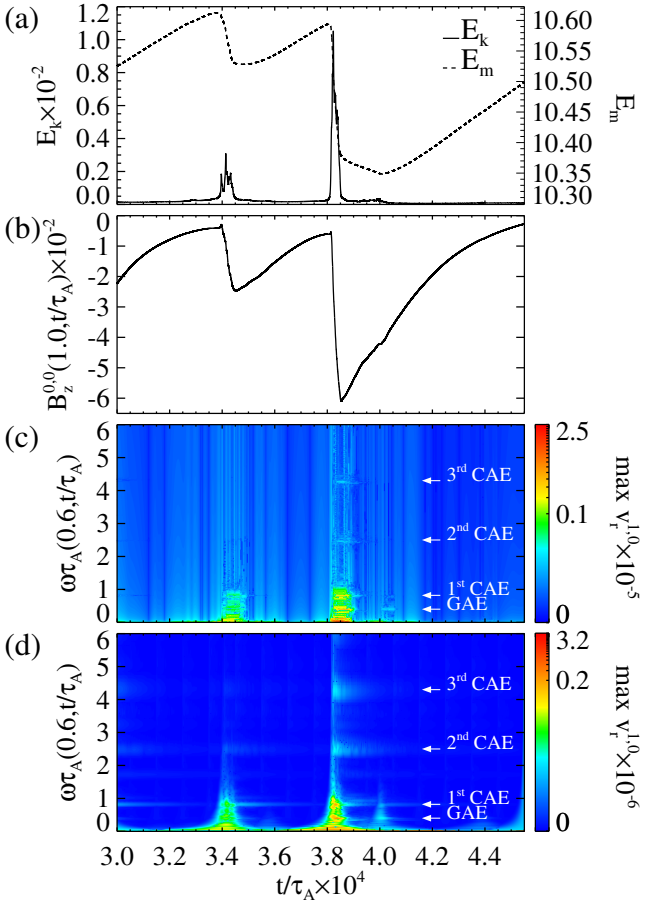

Figure 10: Results of the numerical simulation with time-evolving RFP magnetic filed and RFX-mod-like hollow density profile. $(m,n) = (1,0)$ mode. a) The time trace of the normalized kinetic energy E_k and normalized magnetic energy E_m. b) The time trace of the normalized magnetic field component $B_z^{0,0}$ at a fixed radius $r/a = 1.0$. c)-d) Respectively FFT and CWT showing the time evolution of the frequency spectrum of the normalized velocity field component $v_r^{1,0}$ at a fixed radius $r/a = 0.6$. For the corresponding movie of the second magnetic reconnection event, see supplemental material S4.

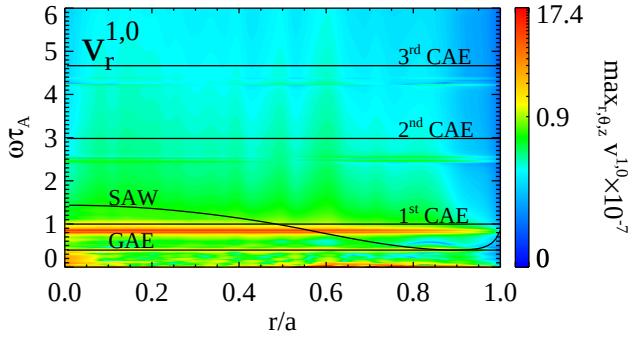

Figure 11: Time-evolving RFP magnetic filed and RFX-mod-like hollow density profile. Verification of frequency spectrum, obtained with FFT, right after the stronger magnetic reconnection event ($\Delta t = (3.90 - 3.95) \times 10^4 \tau_A$ with respect to Fig. (10)) with the theoretical model for the $v_r^{1,0}$ velocity field component. The color scale has been adjusted, compared to Fig. (10), to better highlight the presence of the GAE.

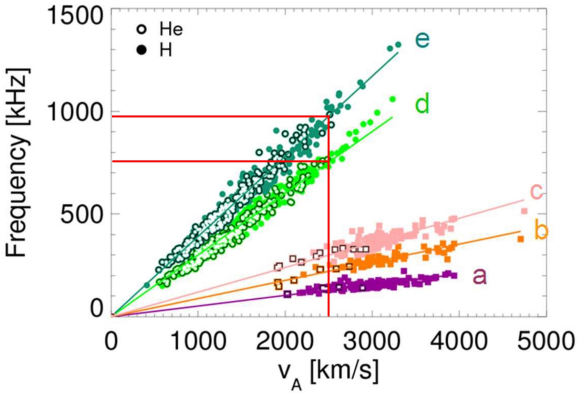

Figure 12: Relation between modes frequency and Alfvén velocity for a large database of H and He plasmas (as also discussed in Ref. [41]). The frequencies for peaks *d* and *e* corresponding to the Alfvén velocity $v_A = 2500$ km/s are marked in red.

for the determination of the triggering mechanism of Alfvén waves in RFP plasmas. Indeed we demonstrated that the Alfvén waves are excited by periodic magnetic reconnection events. In fact the Alfvén activity, composed of SAW, CAEs and GAE, show clear bursts during these events. The GAE, in particular, is observed even with RFX-mod-like hollow density profile.

Finally we used the time-evolving RFP simulation case for the qualitative comparison and theoretical interpretation of the experimentally observed Alfvén waves during the full discharge duration in the RFX-mod device. We compared the numerical spectrum from the fully-3D RFP simulation with hollow density profile, with the RFX-mod one, and we showed a good qualitative agreement between the two. This allowed us to propose the identification of the experimental coherent Alfvén modes (namely the d and e peaks in the experimental spectrum) as a GAE and the 1^{st} CAE, respectively.

Early theoretical work on GAEs was prompted largely by the possibility that they could provide an alternative radio requency heating scheme [70,71]. Appert *et al* [71] concluded that the most efficient such scheme would be one involving antenna excitation of GAEs with $n = 0$. The results of this paper indicate that this is also the GAE most likely to be generated spontaneously in RFP ohmic plasmas.

As mentioned in section 5, the experimental Alfvén waves that are present during the full discharge duration

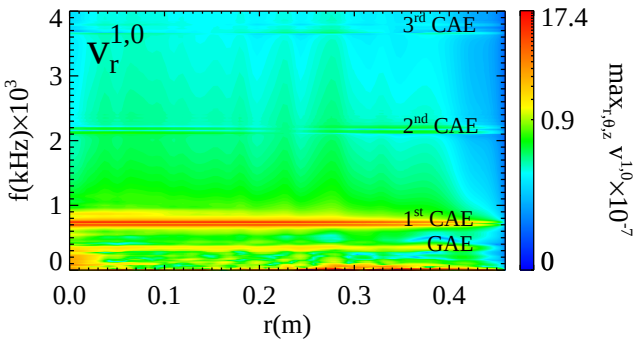

Figure 13: Same frequency spectrum as in Fig.(11), but in physical units by taking $v_A = 2500$ km/s and a minor radius of RFX-mod $a = 0.459$ m.

(*d* and *e* peaks) do not show a significant damping in time, while the numerical one are excited only during the reconnection events, after which they decay more or less quickly in time, especially in case of the hollow-like density profile because of resonance absorption. It is worth noting that we used higher resistivity and viscosity values compared to those estimated experimentally [72] and this contributes to a stronger damping of the Alfvénic modes in between the magnetic reconnection events in our simulation than in the experiment.

In our study we could not reproduce the three lower frequency experimental peaks (*a*, *b* and *c*) observed only during the improved confinement quasi-helical states. This can be due to approximations of the employed numerical model, which neglects toroidal, finite beta and kinetic effects. A toroidal geometry and finite beta would allow for the TAE and the BAE gaps to be excited, with frequencies below the GAE one [63,73], by either energetic particle tails (observed in past studies in RFX-mod plasmas, for which a wave-particle interaction model was proposed [44]) or other mechanisms. Maraschek *et al* [74] proposed the role of the inverse energy cascades on the coupled drift Alfvén small-scalle turbulence to explain the observation of TAEs in ohmically heated tokamak plasmas. Such a coupling has also been identified in the edge region of the RFX-mod plasmas in the form of drift Alfvén vortex structures [75], so that the role of TAEs excitation played by the inverse cascade also for RFX-mod plasmas cannot be excluded. Similarly BAEs destabilization by resonant magnetic perturbations in Ohmic discharges in J-TEXT tokamak have also been observed [73]. Furthermore it was shown [76,77] that the coupling of pressure gradient and the averaged magnetic curvature is important and favorable to the existence of the RSAE, more so in RFP configuration due to the low q value [39] and the possible identification of experimental peaks *a*, *b* and *c* as RSAEs has been speculated [41].

The inclusion of the above-mentioned physical effects presently not taken into account (e.g., finite beta, toroidal geometry and the coupling with fast particles) needs to be addressed in the future. However, in this paper we have shown how rich and articulated is the physics already supported by the "minimum" visco-resistive MHD model presently used. In particular, the excitation mechanism of AEs based on magnetic reconnection events, investigated in this paper, looks like a fundamental phenomenon expected to remain present in a more complete modeling, as well. To this respect, we are currently investigating an analogous mechanism of excitation of Alfvén waves in tokamak plasmas by the sawtooth instability and we plan to address this topic in a future paper.

Acknowledgments

The auhors would like to thank Sergio Briguglio, Liu Chen, Dominique Escande, Matthias Hoelzl, Cristel Krombé, Zhixin Lu, Eric Nardon, Fabio Sattin, Gregorio Vlad and Fulvio Zonca for useful discussions and suggestions, and the whole RFX team for the realization of the experiments discussed in this paper. This work has been carried out within the framework of the EUROfusion Consortium, funded by the European Union via the Euratom Research and Training Programme (Grant Agreement No 101052200 — EUROfusion). Views and opinions expressed are however those of the authors only and do not necessarily reflect those of the European Union or the European Commission. Neither the European Union nor the European Commission can be held responsible for them.

Authors contributions

A. K. and D. B. jointly conceived this paper, in close collaboration with S. C. (who encouraged the study of Alfvénic modes with the SpeCyl code) and M. V.. M. Z. provided data from RFX-mod experiments and support for the experimental comparison of modelling results.

References

[1] N.F. Cramer. *The physics of Alfvén waves*. Wiley-VCH, 2001.

[2] Liu Chen and Fulvio Zonca. "Physics of Alfvén waves and energetic particles in burning plasmas". In: *Rev. Mod. Phys.* **88** (1 2016), p. 015008.

[3] D. A. Dippolito and J. P. Goedbloed. "Mode coupling in a toroidal sharp-boundary plasma. I. Weak-coupling limit". In: *Plasma Physics* **22**.12 (Dec. 1980), pp. 1091–1107.

[4] B. van der Holst, A. J. C. Beliën, and J. P. Goedbloed. "New Alfvén Continuum Gaps and Global Modes Induced by Toroidal Flow". In: *Phys. Rev. Lett.* **84** (13 2000), pp. 2865–2868.

[5] A. Donne and Y. Liang. "MHD control in burning plasmas". In: *Nuclear Fusion* **52** (July 2012).

[6] ITER Physics Expert Group on Energe Drive and ITER Physics Basis Editors. "Chapter 5: Physics of energetic ions". In: *Nuclear Fusion* **39**.12 (1999), pp. 2471–2495.

[7] M. N. Rosenbluth et al. "Energetic Particle Stabilization of Ballooning Modes in Tokamaks". In: *Phys. Rev. Lett.* **51** (21 1983), pp. 1967–1970.

[8] R. B. White, M. N. Bussac, and F. Romanelli. "High-β, Sawtooth-Free Tokamak Operation Using Energetic Trapped Particles". In: *Phys. Rev. Lett.* **62** (5 1989), pp. 539–542.

[9] H. A. Holties et al. "Determination of local tokamak parameters by magnetohydrodynamic spectroscopy". In: *Physics of Plasmas* **4**.3 (1997), pp. 709–719.

[10] J. Vaclavik and K. Appert. "Theory of plasma heating by low frequency waves: Magnetic pumping and Alfvén resonance heating". In: *Nuclear Fusion* **31**.10 (1991), pp. 1945–1997.

[11] S Poedts et al. "Damping of global Alfven waves in tokamaks due to resonant absorption". In: *Plasma Physics and Controlled Fusion* **34**.8 (1992), pp. 1397–1422.

[12] L Villard et al. "Alfvén wave heating and stability". In: *Physica Scripta* **T60** (1995), pp. 44–56.

[13] C.E. Parnell and I. De Moortel. "A contemporary view of coronal heating". In: *Philosophical Transactions of the Royal Society A: Mathematical, Physical and Engineering Sciences* **370**.1970 (2012), 3217–3240.

[14] D.F. Escande, V. Gondret, and F. Sattin. "Relevant heating of the quiet solar corona by Alfvén waves: a result of adiabaticity breakdown". In: *Scientific Reports* **9** (Oct. 2019), p. 14274.

[15] F. Stefani et al. "Mode Conversion and Period Doubling in a Liquid Rubidium Alfvén-Wave Experiment with Coinciding Sound and Alfvén Speeds". In: *Phys. Rev. Lett.* **127** (27 2021), p. 275001.

[16] Allen H. Boozer. "Flattening of the tokamak current profile by a fast magnetic reconnection with implications for the solar corona". In: *Physics of Plasmas* **27**.10 (2020), p. 102305.

[17] L. Chang et al. "Compressional Alfvén eigenmodes excited by runaway electrons". In: *Nuclear Fusion* **61**.3 (2021), p. 036011.

[18] M. Garcia-Munoz et al. "Active control of Alfvén eigenmodes in magnetically confined toroidal plasmas". In: *Plasma Physics and Controlled Fusion* **61**.5 (2019), p. 054007.

[19] B.N. Breizman and S.E. Sharapov. "Energetic particle drive for toroidicity-induced Alfven eigenmodes and kinetic toroidicity-induced Alfven eigenmodes in a low-shear tokamak". In: *Plasma Physics and Controlled Fusion* **37**.10 (1995), pp. 1057–1074.

[20] S.E. Sharapov et al. "Energetic particle instabilities in fusion plasmas". In: *Nuclear Fusion* **53**.10 (2013), p. 104022.

[21] N. Nakajima, C. Z. Cheng, and M. Okamoto. "High-n helicity-induced shear Alfvén eigenmodes". In: *Physics of Fluids B: Plasma Physics* **4**.5 (1992), pp. 1115–1121.

[22] S. Yamamoto et al. "Observation of Helicity-Induced Alfvén Eigenmodes in Large-Helical-Device Plasmas Heated by Neutral-Beam Injection". In: *Phys. Rev. Lett.* **91** (24 2003), p. 245001.

[23] D. A. Spong, R. Sanchez, and A. Weller. "Shear Alfvén continua in stellarators". In: *Physics of Plasmas* **10**.8 (2003), pp. 3217–3224.

[24] A. D. Turnbull et al. "Global Alfvén modes: Theory and experiment*". In: *Physics of Fluids B: Plasma Physics* **5**.7 (1993), pp. 2546–2553.

[25] W. W. Heidbrink et al. "Observation of beta-induced Alfvén eigenmodes in the DIII-D tokamak". In: *Phys. Rev. Lett.* **71** (6 1993), pp. 855–858.

[26] D.A. Spong. "Simulation of Alfvén frequency cascade modes in reversed shear-discharges using a Landau-closure model". In: *Nuclear Fusion* **53**.5 (2013), p. 053008.

[27] W.W. Heidbrink et al. "The effect of the fast-ion profile on Alfvén eigenmode stability". In: *Nuclear Fusion* **53**.9 (2013), p. 093006.

[28] C. R. Cook et al. "Identification of island-induced Alfvén eigenmodes in a reversed field pinch". In: *Plasma Physics and Controlled Fusion* **58**.5 (2016), p. 054004.

[29] L. Chen and F. Zonca. "Nonlinear equilibria, stability and generation of zonal structures in toroidal plasmas". In: *Nuclear Fusion* **47**.8 (2007), pp. 886–891.

[30] Z. Chang et al. "Alfven frequency modes at the edge of TFTR plasmas". In: *Nuclear Fusion* **35**.12 (1995), pp. 1469–1479.

[31] Maraschek M. *et al*. In: *Proc. 24th Eur. Conf. on Controlled Fusion and Plasma Physics (Berchtesgaden, 1997)* **21A** (1997), p. 1525.

[32] A. Sykes. "Overview of recent spherical tokamak results". In: *Plasma Physics and Controlled Fusion* **43**.12A (2001), A127–A139.

[33] K. Mcclements et al. "Excitation of axisymmetric Alfvénic modes in Ohmic tokamak discharges". In: *Nuclear Fusion* **42** (Aug. 2002), p. 1155.

[34] Giorgio Regnoli et al. "Observations of toroidicity-induced Alfvén eigenmodes in a reversed field pinch plasma". In: *Physics of Plasmas* **12** (Apr. 2005).

[35] S. Spagnolo et al. "Alfvén eigenmodes in the RFX-mod reversed-field pinch plasma". In: *Nuclear Fusion* **51**.8 (2011), p. 083038.

[36] J. J. Koliner et al. "Fast-Particle-Driven Alfvénic Modes in a Reversed Field Pinch". In: *Phys. Rev. Lett.* **109** (11 2012), p. 115003.

[37] L. Lin et al. "Energetic-particle-driven instabilities and induced fast-ion transport in a reversed field pinch". In: *Physics of Plasmas* **21**.5 (2014), p. 056104.

[38] P. J. Bonofiglo et al. "Fast ion transport in the quasi-single helical reversed-field pinch". In: *Physics of Plasmas* **26**.2 (2019), p. 022502.

[39] H. Cai et al. "Effects of pressure gradient on global Alfvén eigenmodes in reversed field pinch". In: *Physics of Plasmas* **21**.2 (2014), p. 022513.

[40] M. Li et al. "Alfvén modes in the Madison Symmetric Torus". In: *Physics of Plasmas* **21**.8 (2014), p. 082505.

[41] S. Spagnolo et al. "Alfvén Eigenmodes in the RFX-mod reversed-field pinch plasma". In: *37th EPS Conference on Plasma Physics* (Dublin, Ireland). Vol. 34A. 2010, P4.162.

[42] S. Cappello and D. F. Escande. "Bifurcation in Viscoresistive MHD: The Hartmann Number and the Reversed Field Pinch". In: *Phys. Rev. Lett.* **85** (18 2000), pp. 3838–3841.

[43] R. Lorenzini et al. "Self-organized helical equilibria as a new paradigm for ohmically heated fusion plasmas". In: *Nature Physics* **5** (June 2009), pp. 570–574.

[44] S. Costa et al. "A wave-particle interaction model for tail ion acceleration in reversed field pinch plasmas". In: *Plasma Physics and Controlled Fusion* **41**.12 (1999), pp. 1485–1496.

[45] R. M. Magee et al. "Anisotropic Ion Heating and Tail Generation during Tearing Mode Magnetic Reconnection in a High-Temperature Plasma". In: *Phys. Rev. Lett.* **107** (6 2011), p. 065005.

[46] V. A. Svidzinski et al. "Modeling of ion heating from viscous damping of reconnection flows in the reversed field pinch". In: *Physics of Plasmas* **15**.6 (2008), p. 062511.

[47] M. Gobbin et al. "Ion heating and energy balance during magnetic reconnection events in the RFX-mod experiment". In: *Nuclear Fusion* **62**.2 (2022), p. 026030.

[48] S. Cappello and D. Biskamp. "Reconnection processes and scaling laws in reversed field pinch magnetohydrodynamics". In: *Nuclear Fusion* **36**.5 (1996), p. 571.

[49] D. Bonfiglio et al. "Experimental-like Helical Self-Organization in Reversed-Field Pinch Modeling". In: *Phys. Rev. Lett.* **111** (8 2013), p. 085002.

[50] L. Chacón. "An optimal, parallel, fully implicit Newton–Krylov solver for three-dimensional viscoresistive magnetohydrodynamics". In: *Physics of Plasmas* **15**.5 (2008), p. 056103.

[51] D. Bonfiglio, L. Chacón, and S. Cappello. "Nonlinear three-dimensional verification of the SPECYL and PIXIE3D magnetohydrodynamics codes for fusion plasmas". In: *Physics of Plasmas* **17**.8 (2010), p. 082501.

[52] M. Veranda et al. "Magnetohydrodynamics modelling successfully predicts new helical states in reversed-field pinch fusion plasmas". In: *Nuclear Fusion* **57**.11 (2017), p. 116029.

[53] W. Park et al. "Plasma simulation studies using multilevel physics models". In: *Physics of Plasmas* **6**.5 (1999), pp. 1796–1803.

[54] X. Wang et al. "An extended hybrid magnetohydrodynamics gyrokinetic model for numerical simulation of shear Alfvén waves in burning plasmas". In: *Physics of Plasmas* **18**.5 (2011), p. 052504.

[55] X. Wang et al. "Analysis of the nonlinear dynamics of a chirping-frequency Alfvén mode in a tokamak equilibrium". In: *Physics of Plasmas* **29**.3 (2022), p. 032512.

[56] G. Fogaccia, G. Vlad, and S. Briguglio. "Linear benchmarks between the hybrid codes HYMAGYC and HMGC to study energetic particle driven Alfvénic modes". In: *Nuclear Fusion* **56**.11 (2016), p. 112004.

[57] G. Vlad et al. “A linear benchmark between HYMAGYC, MEGA and ORB5 codes using the NLED-AUG test case to study Alfvénic modes driven by energetic particles”. In: *Nuclear Fusion* **61**.11 (2021), p. 116026.

[58] Y. Todo. “Properties of energetic-particle continuum modes destabilized by energetic ions with beam-like velocity distributions”. In: *Physics of Plasmas* **13**.8 (2006), p. 082503.

[59] Yawei Hou et al. “NIMROD calculations of energetic particle driven toroidal Alfvén eigenmodes”. In: *Physics of Plasmas* **25**.1 (2018), p. 012501.

[60] A. Dvornova et al. “Modeling of TAE mode excitation with an antenna in realistic X-point geometry”. In: *Physics of Plasmas* **27**.1 (2020), p. 012507.

[61] M. Hoelzl et al. “The JOREK non-linear extended MHD code and applications to large-scale instabilities and their control in magnetically confined fusion plasmas”. In: *Nuclear Fusion* **61**.6 (2021), p. 065001.

[62] D. Bonfiglio et al. “Necessary criterion for magnetic field reversal in the reversed-field pinch”. In: *Nuclear Fusion* **51**.6 (2011), p. 063016.

[63] L. Villard and J. Vaclavik. “Alfven frequency modes and global Alfven eigenmodes”. In: *Nuclear Fusion* **37**.3 (1997), p. 351.

[64] R. Ochoukov et al. “High frequency Alfvén eigenmodes detected with ion-cyclotron-emission diagnostics during NBI and ICRF heated plasmas on the ASDEX Upgrade tokamak”. In: *Nuclear Fusion* **60**.12 (2020), p. 126043.

[65] H. Kimura et al. “Alfvén eigenmode and energetic particle research in JT-60U”. In: *Nuclear Fusion* **38**.9 (1998), pp. 1303–1314.

[66] T. E. Evans et al. “Direct Observation of the Structure of Global Alfvén Eigenmodes in a Tokamak Plasma”. In: *Phys. Rev. Lett.* **53** (18 1984), pp. 1743–1746.

[67] D. F. Escande et al. “Single helicity: a new paradigm for the reversed field pinch”. In: *Plasma Physics and Controlled Fusion* **42**.12B (2000), B243.

[68] A. Hasegawa and L. Chen. “Kinetic processes in plasma heating by resonant mode conversion of Alfvén wave”. In: *The Physics of Fluids* **19**.12 (1976), pp. 1924–1934.

[69] M. Veranda et al. “Magnetic reconnection in three-dimensional quasi-helical pinches”. In: *Rendiconti Lincei. Scienze Fisiche e Naturali* **31** (Aug. 2020).

[70] S. M. Mahajan, David W. Ross, and Gwo-Liang Chen. “Discrete Alfvén eigenmode spectrum in magnetohydrodynamics”. In: *The Physics of Fluids* **26**.8 (1983), pp. 2195–2199.

[71] K. Appert et al. “Heating in Toroidal Plasmas”. In: *Report on the Third Joint Varenna-Grenoble International Symposium* (Grenoble, France). 1982, P203.

[72] P. Piovesan et al. “Magnetic order and confinement improvement in high-current regimes of RFX-mod with MHD feedback control”. In: *Nuclear Fusion* **49** (July 2009), p. 085036.

[73] Linzi Liu et al. “Beta-induced Alfvén eigenmodes destabilized by resonant magnetic perturbations in the J-TEXT tokamak”. In: *Nuclear Fusion* **59**.12 (2019), p. 126022.

[74] M. Maraschek et al. “Observation of Toroidicity-Induced Alfvén Eigenmodes in Ohmically Heated Plasmas by Drift Wave Excitation”. In: *Phys. Rev. Lett.* **79** (21 1997), pp. 4186–4189.

[75] N. Vianello et al. “Drift-Alfvén vortex structures in the edge region of a fusion relevant plasma”. In: *Nuclear Fusion* **50**.4 (2010), p. 042002.

[76] B. N. Breizman, M. S. Pekker, and S. E. Sharapov. “Plasma pressure effect on Alfvén cascade eigenmodes”. In: *Physics of Plasmas* **12**.11 (2005), p. 112506.

[77] G. Y. Fu and H. L. Berk. “Effects of pressure gradient on existence of Alfvén cascade modes in reversed shear tokamak plasmas”. In: *Physics of Plasmas* **13**.5 (2006), p. 052502.